Applied Catalysis B: Environmental 93 (2009) 194–204

Contents lists available at ScienceDirect

Applied Catalysis B: Environmental

journal homepage: www.elsevier.com/locate/apcatb

Effect of manganese substitution on the structure and activity of iron titanate catalyst for the selective catalytic reduction of NO with NH_3

Fudong Liu, Hong He *, Yun Ding, Changbin Zhang

State Key Laboratory of Environmental Chemistry and Ecotoxicology, Research Center for Eco-Environmental Sciences, Chinese Academy of Sciences, Beijing 100085, PR China

ARTICLE INFO

Article history:
Received 9 June 2009
Received in revised form 10 September 2009
Accepted 22 September 2009
Available online 25 September 2009

Keywords:
Selective catalytic reduction
Iron titanate catalyst
Mn substitution amounts
Low temperature activity
Redox behavior

ABSTRACT

Selective catalytic reduction (SCR) of NO with NH_3 over manganese substituted iron titanate catalysts was fully studied. The low temperature SCR activity was greatly enhanced when partial Fe was substituted by Mn, although the N_2 selectivity showed some decrease to a certain extent. The Mn substitution amounts showed obvious influence on the catalyst structure, redox behavior and NH_3/NO_x adsorption ability of the catalysts. Among $Fe_aMn_{1-a}TiO_x$ (a = 1, 0.75, 0.5, 0.2, 0) serial catalysts, $Fe_{0.5}Mn_{0.5}TiO_x$ with the molar ratio of Fe:Mn = 1:1 showed the highest SCR activity, because the interaction of iron, manganese and titanium species in this catalyst led to the largest surface area and the highest porosity, the severest structural distortion and most appropriate structural disorder, the enhanced oxidative ability of manganese species, the highest mobility of lattice oxygen, the proper ratio of Brønsted acid sites and Lewis acid sites together with the enhanced NO_x adsorption capacity.

1. Introduction

Selective catalytic reduction (SCR) of NO with NH_3 is one of the most efficient and economic technologies for the removal of nitrogen oxides (NO_x) from stationary and mobile sources, and the most widely used catalyst system is V_2O_5–WO_3 (MoO_3)/TiO_2 [1]. Because of some inevitable disadvantages in practical application, such as the narrow operation temperature window [2], high conversion of SO_2 to SO_3 at high temperatures [3] and the toxicity of vanadium pentoxide to environment and human health [4], more and more researchers are focusing on the development of new SCR catalysts. In our previous study [5,6], we have developed an environmentally friendly novel iron titanate catalyst in crystallite phase with specific Fe–O–Ti structure, which showed excellent SCR activity, N_2 selectivity and H_2O/SO_2 durability in the medium temperature range. However, the catalytic activity was not high enough for the application in denitrogenation of exhaust gas with low temperature, such as the flue gas after dust removal and desulfurization from coal-fired power plants and the exhaust gas from diesel engines in cold-start process. Therefore, it is very necessary to modify this iron titanate catalyst to improve the low temperature activity, which is crucial for the practical utilization.

Manganese oxides usually show good SCR activity in the low temperature range, such as pure MnO_x [7,8], MnO_x loaded on TiO_2/Al_2O_3/SiO_2/AC (activated carbon) [9–12] and Mn–Ce, Mn–Cu mixed oxides [13–15]. Previous studies showed that in Fe-containing SCR catalysts, the introduction of Mn could obviously enhance the low temperature activity [16,17], probably due to the synergistic effect between iron and manganese species. It was reported that the introduction of lanthanide elements (such as La, Ce and Pr) and the third main group element In could also improve the activity, stability or SO_2 durability of the SCR catalysts using NH_3 or hydrocarbons as reducing agent [18–22]. Therefore, based on our iron titanate catalyst, we can also substitute partial Fe by other elements to adjust its physicochemical properties, expecting to enhance the low temperature SCR activity.

In this paper, five kinds of elements including La, Ce, Pr, In and Mn were introduced into the iron titanate catalyst, among which Mn showed the best promoting effect. Based on this result, we further investigated the influence of Mn substitution amounts on the catalyst structure and catalytic activity using various characterization methods. The structural properties were characterized using N_2 physisorption, powder X-ray diffraction (XRD) and X-ray absorption fine structure (XAFS) methods. Then, X-ray photoelectron spectra (XPS) and H_2-temperature programmed reduction (H_2-TPR) were conducted to evaluate the variation of redox properties during the substitution process. Finally, temperature programmed desorption of NH_3 and NO_x (NH_3-TPD and NO_x-TPD) together with in situ diffuse reflectance infrared Fourier transform spectroscopy (in situ DRIFTS) of NH_3 and NO_x adsorption was carried out to reveal the evolution of adsorption ability of reactants, which is important for the SCR reaction. The promoting mechanism of Mn on the low temperature SCR activity of iron titanate catalyst was proposed accordingly.

* Corresponding author at: P.O. Box 2871, 18 Shuangqing Road, Haidian District, Beijing 100085, PR China. Tel.: +86 10 62849123; fax: +86 10 62849123.
E-mail address: honghe@rcees.ac.cn (H. He).

0926-3373/$ – see front matter © 2009 Elsevier B.V. All rights reserved.
doi:10.1016/j.apcatb.2009.09.029

2. Experimental

2.1. Catalyst synthesis and activity test

$Fe_{0.9}M_{0.1}TiO_x$ (M = La, Ce, Pr, In, Mn) and $Fe_aMn_{1-a}TiO_x$ with different Mn substitution amounts (a = 1, 0.75, 0.5, 0.2, 0) were prepared by co-precipitation method using $Fe(NO_3)_3{\cdot}9H_2O$, $Ti(SO_4)_2$, relevant metal nitrates as precursors and $NH_3{\cdot}H_2O$ (25 wt%) as precipitator. The precipitate cake was filtrated and washed using distilled water, followed by desiccation at 100 °C for 12 h and calcination at 400 °C for 6 h in air condition. Pure oxides including Fe_2O_3, MnO_x and TiO_2 were prepared from $Fe(NO_3)_3{\cdot}9H_2O$, $Mn(NO_3)_2$ and $Ti(SO_4)_2$ using the same precipitation method for the comparison of SCR activity. The state-of-the-art SCR catalyst 4.5 wt% V_2O_5–10 wt% WO_3/TiO_2 was also prepared using conventional wet impregnation method as reference in the SCR activity test.

The NH_3-SCR, NO oxidation and NH_3 oxidation tests were carried out over 0.6 ml catalysts (ca. 200–350 mg due to the different catalyst densities) in a fixed-bed quartz tube reactor and the reaction conditions were as follows: 500 ppm NO and (or) 500 ppm NH_3, 5 vol.% O_2, 1000 ppm CO (when used), 5 vol.% CO_2 (when used), 5 vol.% H_2O (when used), N_2 balance and gas hourly space velocity (GHSV) = 50 000 h^{-1}. The effluent gas was analyzed using an FTIR spectrometer (Nicolet Nexus 670) equipped with a heated, low volume multiple-path gas cell (2 m). NO_x conversion (X_{NO_x}) and N_2 selectivity (S_{N_2}) were calculated as follows:

$$X_{NO_x} = \left(1 - \frac{[NO_x]_{out}}{[NO_x]_{in}}\right) \times 100\% \text{ with } [NO_x] = [NO] + [NO_2] \quad (1)$$

$$S_{N_2} = \frac{[NO]_{in} + [NH_3]_{in} - [NO_2]_{out} - 2[N_2O]_{out}}{[NO]_{in} + [NH_3]_{in}} \times 100\% \quad (2)$$

2.2. Characterizations

N_2 adsorption–desorption isotherms were obtained at 77 K using a Quantachrome Autosorb-1C instrument. Prior to N_2 adsorption, the samples were degassed at 300 °C for 4 h. The surface areas were determined by BET equation in 0.05–0.35 partial pressure range. The pore volumes, average pore diameters and pore size distributions were determined by BJH method from the desorption branches of the isotherms.

Powder XRD measurements were carried out on a computerized Rigaku D/max-RB Diffractometer (Japan, Cu K_α as radiation resource). The data of 2θ from 10° to 90° were collected at 4 °/min with the stepsize of 0.02°.

XAFS experiments were implemented on U7C beamline of National Synchrotron Radiation Laboratory (NSRL), of which the storage ring was operated at 0.8 GeV with a maximum current of 300 mA. The hard X-ray beam was from a three-pole superconducting Wiggler with a magnetic field intensity of 6 T. A fixed-exit Si(1 1 1) double-crystal monochromator was used to reduce the harmonic content of the monochrome beam. The incident and output beam intensities were monitored and recorded using ionization chambers filled by Ar/N_2. A Keithley Model 6517 Electrometer was used to collect the electron charge directly. Before XAFS measurement, the catalyst samples were crushed into fine powder above 200 mesh and coated onto transparent adhesive tapes. The XAFS spectra (X-ray absorption near-edge spectroscopy, XANES and extended X-ray absorption fine-structure spectroscopy, EXAFS) of Fe-K-edge and Mn-K-edge were recorded in transmission mode at room temperature in air condition. The collected XAFS data were calibrated according to standard Fe_2O_3 and MnO_2 samples and then analyzed using Viper software package according to standard procedures [23]. During the EXAFS data processing procedure, the back-subtracted EXAFS function was firstly converted into k space and weighted by k^3 in order to compensate for the diminishing amplitude because of the decay of the photoelectron wave. The Fourier transforming of the k^3-weighted EXAFS data was performed in the range of k = 2–11.01 $Å^{-1}$ for both Fe-K-edge and Mn-K-edge with a Hanning function window.

XPS were recorded on a Scanning X-ray Microprobe (PHI Quantera, ULVAC-PHI, Inc.) using Al K_α radiation (1486.7 eV). Binding energies of Fe 2p, Mn 2p, Ti 2p and O 1s were calibrated using C 1s peak (BE = 284.8 eV) as standard.

Prior to H_2-TPR experiment, the samples (100 mg) were pretreated at 300 °C in a flow of 20 vol.% O_2/He (30 ml/min) for 0.5 h and cooled down to the room temperature (30 °C). Then the temperature was raised linearly to 900 °C at the rate of 10 °C/min in a flow of 5 vol.% H_2/Ar (30 ml/min). The H_2 signal (m/z = 2) was monitored online using a quadrupole mass spectrometer (HPR20, Hiden Analytical Ltd.).

NH_3-TPD and NO_x-TPD were also performed using the same quadrupole mass spectrometer to record the signals of NH_3 (m/z = 16 for NH_2 and m/z = 15 for NH) and NO_x (m/z = 30 for NO and m/z = 46 for NO_2). Prior to TPD experiments, the samples (100 mg) were also pretreated at 300 °C in a flow of 20 vol.% O_2/He (30 ml/min) for 0.5 h and cooled down to the room temperature (30 °C). Then the samples were exposed to a flow of 2500 ppm NH_3/Ar or 2500 ppm NO + 10 vol.% O_2/Ar (30 ml/min) at 30 °C for 1 h, following by Ar purge for another 1 h. Finally, the temperature was raised to 500 °C in Ar flow at the rate of 10 °C/min.

The in situ DRIFTS experiments of NH_3/NO_x adsorption over $Fe_aMn_{1-a}TiO_x$ catalysts were performed on an FTIR spectrometer (Nicolet Nexus 670) equipped with an MCT/A detector cooled by liquid nitrogen. An in situ DRIFTS reactor cell with ZnSe window (Nexus Smart Collector) connected to a purging/adsorption gas control system was used for the NH_3/NO_x in situ adsorption experiments. The temperature of the reactor cell was controlled precisely by an Omega programmable temperature controller. Prior to NH_3/NO_x adsorption, the samples were pretreated at 400 °C in a flow of 20 vol.% O_2/N_2 for 0.5 h and cooled down to 30 °C. The spectra of different catalysts at 30 °C were collected in flowing N_2 and set as backgrounds, which were automatically subtracted from the final spectra after NH_3/NO_x adsorption. Then the samples were exposed to a flow of 500 ppm NH_3/N_2 or 500 ppm NO + 5 vol.% O_2/N_2 (300 ml/min) at 30 °C for 1 h, following by N_2 purge for another 0.5 h. All spectra were recorded by accumulating 100 scans with a resolution of 4 cm^{-1}.

3. Results and discussion

3.1. Catalytic performance

3.1.1. SCR activity of $Fe_{0.9}M_{0.1}TiO_x$ catalysts (M = La, Ce, Pr, In, Mn)

Fig. 1 shows the NO_x conversion as a function of temperature in the NH_3-SCR reaction over $Fe_{0.9}M_{0.1}TiO_x$ catalysts (M = La, Ce, Pr, In, Mn). From the results we can see that, the substitution of partial Fe with other elements could indeed influence the SCR activity of iron titanate catalyst. At temperatures below 250 °C, the Mn and Ce substitutions could obviously enhance the NO_x conversions, while the La, Pr and In substitutions decreased the NO_x conversions to a certain extent. Moreover, the Ce substitution lowered the NO_x conversion at relatively high temperatures above 300 °C, while the Mn substitution did not show such an obvious negative influence. Therefore, we chose Mn as the substitution element to carry out our further investigations, such as the effect of Mn substitution amounts on NH_3-SCR, NO oxidation and NH_3 oxidation activities, together with the relationship between catalyst structure and catalytic activity.

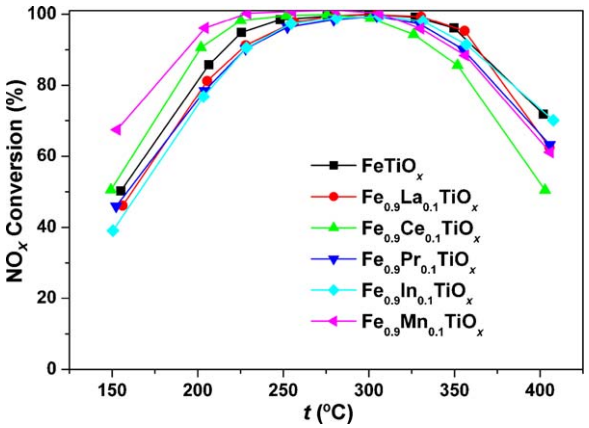

Fig. 1. NO_x conversion as a function of temperature in the NH_3-SCR reaction over $Fe_{0.9}M_{0.1}TiO_x$ catalysts. Reaction conditions: [NO] = [NH_3] = 500 ppm, [O_2] = 5 vol.%, N_2 balance, total flow rate 500 ml/min and GHSV = 50 000 h^{-1}.

3.1.2. SCR activity of $Fe_aMn_{1-a}TiO_x$ catalysts

Fig. 2A shows the results of NO_x conversion and N_2 selectivity in the SCR reaction over $Fe_aMn_{1-a}TiO_x$ (a = 1, 0.75, 0.5, 0.2, 0) catalysts and pure oxides including Fe_2O_3, MnO_x and TiO_2 as a function of temperature from 75 to 400 °C. As we can see, pure TiO_2 showed no SCR activity below 350 °C and only 30% NO_x conversion was obtained at 400 °C. Pure Fe_2O_3 and MnO_x showed very narrow operation temperature windows in the high and low temperature ranges, respectively, and both of the maximum NO_x conversions could not reach 100%. Furthermore, the N_2 selectivity over these two samples was rather low as shown in the inserted figure. The coexistence of Fe and Ti in $FeTiO_x$ greatly enlarged the operation temperature window and the NO_x could be completely reduced from 225 to 350 °C with high N_2 selectivity. When partial Fe was substituted by Mn, the NO_x conversions in the relatively low temperature range had an obvious increase. $Fe_{0.5}Mn_{0.5}TiO_x$ with the molar ratio of Fe:Mn = 1:1 showed the best activity, over which NO_x was completely reduced at about 175 °C. However, the continuing substitution of Fe by more Mn led to an activity decrease, and the NO_x conversions over $Fe_{0.2}Mn_{0.8}TiO_x$ and $MnTiO_x$ from 75 to 250 °C were even lower than that over $Fe_{0.75}Mn_{0.25}TiO_x$. The apparent SCR activity at low temperatures increased in the following sequence: $FeTiO_x \ll MnTiO_x < Fe_{0.2}Mn_{0.8}TiO_x < Fe_{0.75}Mn_{0.25}TiO_x < Fe_{0.5}Mn_{0.5}TiO_x$. In previous study by Qi and Yang [16], they also observed that Fe–Mn/TiO_2 catalyst with Fe:Mn = 1:1 showed the highest activity among their loaded type catalysts in the SCR reaction. This could be attributed to the strong interaction between Fe and Mn which led to high dispersion of active phases and thus the high SCR activity.

Although the substitution of Fe by Mn in iron titanate catalyst could enhance the SCR activity, the N_2 selectivity had an obvious decrease owing to the production of N_2O, especially at high temperatures above 200 °C. The N_2 selectivity at high temperatures decreased in the following sequence: $FeTiO_x > Fe_{0.75}Mn_{0.25}TiO_x > Fe_{0.5}Mn_{0.5}TiO_x \approx Fe_{0.2}Mn_{0.8}TiO_x \approx MnTiO_x$. Considering the NO_x conversion and N_2 selectivity, we chose $Fe_{0.75}Mn_{0.25}TiO_x$ as model catalyst over which the N_2 selectivity could maintain above 90% at temperatures below 300 °C, to compare with the state-of-the-art SCR catalysts including the traditional V_2O_5–WO_3/TiO_2 catalyst and Fe, Cu exchanged zeolites. As shown in Fig. 2B, Fe/ZSM-5 [24] and Fe/HBEA [4] catalysts showed good SCR activity at relatively high temperatures, over which the maximum NO/NO_x conversions were obtained above 350 and 250 °C, respectively. As for our $Fe_{0.75}Mn_{0.25}TiO_x$ catalyst, the low temperature SCR activity was much better than that of Fe exchanged zeolites, although the high temperature SCR activity above 300 °C showed sharp decrease resulting in a narrow operation temperature window. Remarkably,

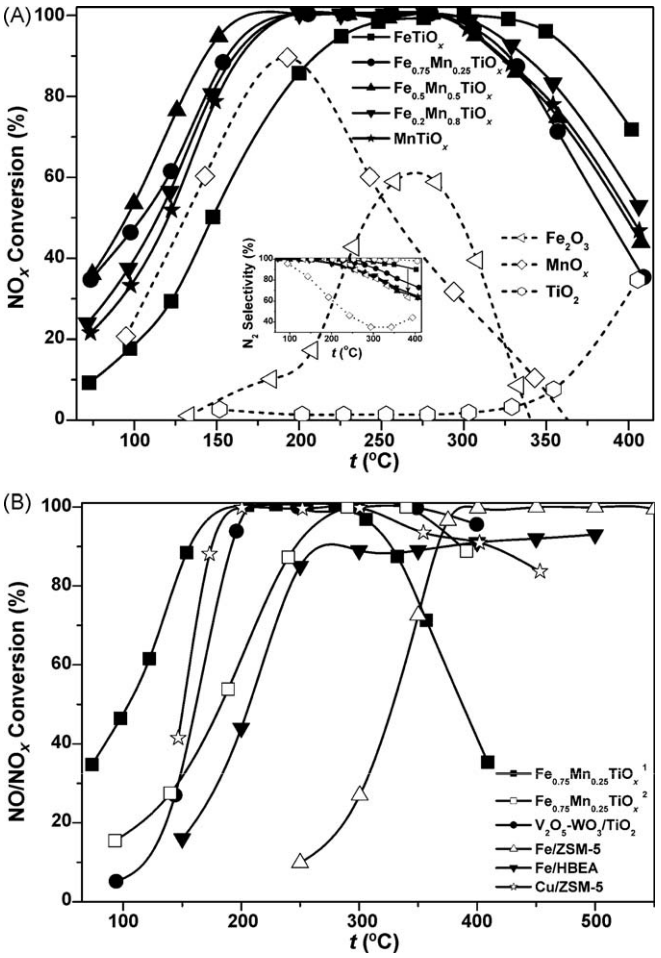

Fig. 2. (A) NO_x conversion and N_2 selectivity (inserted) in the NH_3-SCR reaction over $Fe_aMn_{1-a}TiO_x$ catalysts and pure oxides including Fe_2O_3, MnO_x and TiO_2, reaction conditions: [NO] = [NH_3] = 500 ppm, [O_2] = 5 vol.%, N_2 balance and GHSV = 50 000 h^{-1}. (B) Comparison of apparent SCR activity over $Fe_{0.75}Mn_{0.25}TiO_x$[1] (GHSV = 50 000 h^{-1} without H_2O), $Fe_{0.75}Mn_{0.25}TiO_x$[2] (GHSV = 100 000 h^{-1} with 10 vol.% H_2O), 4.5 wt% V_2O_5–10 wt% WO_3/TiO_2, Fe/ZSM-5 (NO conversion on Fe(58)-ZSM-5(10) from Ref. [24], reaction conditions: [NO] = [NH_3] = 1000 ppm, [O_2] = 2 vol.% and GHSV = 46 000 h^{-1}), Fe/HBEA (NO_x conversion on 0.25Fe/HBEA from Ref. [4], reaction conditions: [NO] = [NH_3] = 500 ppm, [O_2] = 5 vol.% and GHSV = 50 000 h^{-1}) and Cu/ZSM-5 (NO conversion on CuZSM-5-124-fresh from Ref. [25], reaction conditions: [NO] = [NH_3] = 500 ppm, [O_2] = 5 vol.%, [H_2O] = 10 vol.% and GHSV = 100 000 h^{-1}).

the temperature for the 50% NO_x conversion over $Fe_{0.75}Mn_{0.25}TiO_x$ was ca. 50 °C lower than that over the traditional V_2O_5–WO_3/TiO_2 catalyst, making it possible to be utilized for the removal of NO_x from actual flue gas with low exhaust temperature. To fully compare the SCR activity of $Fe_{0.75}Mn_{0.25}TiO_x$ with that of Cu/ZSM-5 reported by Park et al. [25], we also performed another activity test under the identical reaction conditions with those in literature, i.e. GHSV = 100 000 h^{-1} and 10 vol.% H_2O. Under the high GHSV and H_2O concentration, the operation temperature window of $Fe_{0.75}Mn_{0.25}TiO_x$ greatly shifted towards high temperature range, thus resulting in lower SCR activity below 300 °C than that of Cu/ZSM-5. Therefore, GHSV is an important factor to be considered in catalyst design and the H_2O durability of $Fe_{0.75}Mn_{0.25}TiO_x$ still needs to be improved in our future work. Furthermore, the influences of GHSV and O_2 concentration on NO_x conversions over $Fe_{0.75}Mn_{0.25}TiO_x$ were also investigated (Figs. S1 and S2 in Supporting Information). The NO_x conversions over this catalyst still could get 100% above 250 °C even at a high GHSV of 100 000 h^{-1}, which is beneficial to the actual industrial application. The influence of O_2 on NO_x conversions was more obvious at low temperatures than that at

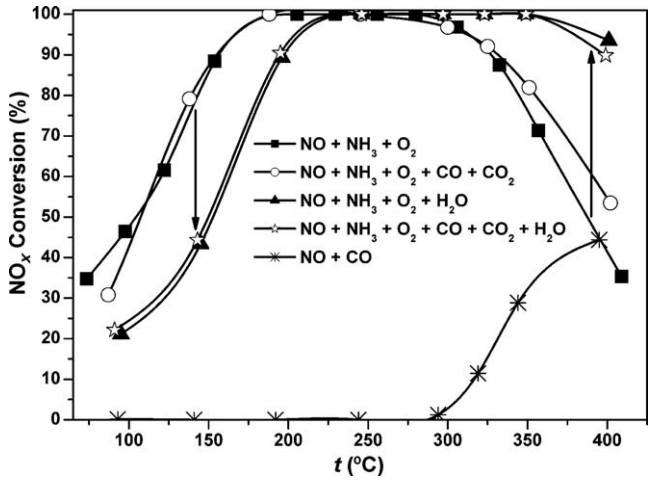

Fig. 3. Influence of CO, CO_2 and H_2O on NO_x conversion in the NH_3-SCR reaction over $Fe_{0.75}Mn_{0.25}TiO_x$ catalyst. Reaction conditions: [NO] = [NH_3] = 500 ppm, [O_2] = 5 vol.%, [CO] = 1000 ppm (when used), [CO_2] = 5 vol.% (when used), [H_2O] = 5 vol.% (when used), N_2 balance, total flow rate 500 ml/min and GHSV = 50 000 h^{-1}.

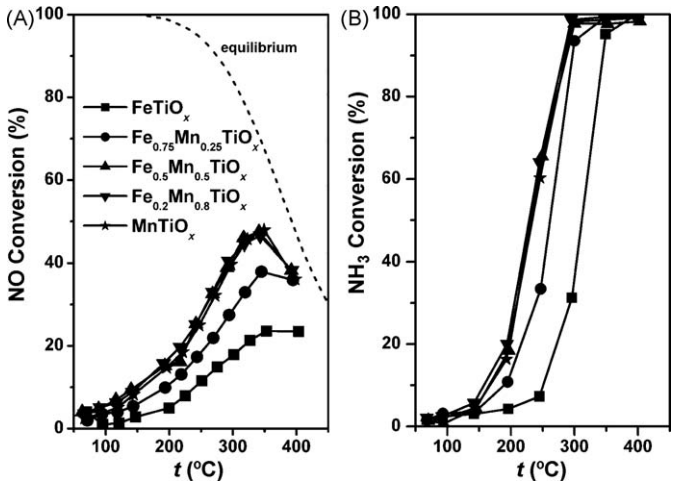

Fig. 4. (A) NO conversion in separate NO oxidation reaction and (B) NH_3 conversion in separate NH_3 oxidation reaction over $Fe_aMn_{1-a}TiO_x$ catalysts. Reaction conditions: [NO] = 500 ppm or [NH_3] = 500 ppm, [O_2] = 5 vol.%, N_2 balance, total flow rate 500 ml/min and GHSV = 50 000 h^{-1}.

high temperatures, implying that different SCR reaction mechanisms might be followed in different temperature ranges, just as those over unsubstituted iron titanate catalyst [26].

3.1.3. Influence of CO, CO_2 and H_2O on the SCR activity

For practical purposes, the $Fe_{0.75}Mn_{0.25}TiO_x$ catalyst was also tested in the presence of CO, CO_2 and H_2O, and the results are shown in Fig. 3. As we can see, the existence of CO and CO_2 in the feeding gas did not obviously influence the SCR activity below 200 °C, which is similar as the results shown by Balle et al. [4]. However, the NO_x conversion above 300 °C showed a slight increase, probably due to the reduction of NO_x by CO when the unselective oxidation of NH_3 severely happened at high temperatures: $2CO + 2NO \rightarrow N_2 + 2CO_2$. To confirm this speculation, additional experiment concerning the reaction between NO and CO was performed, during which partial NO was indeed reduced to N_2 by CO above 300 °C (as shown in Fig. 3). On the other hand, the presence of H_2O in the feeding gas significantly decreased the NO_x conversion below 200 °C mainly due to the blocking of active sites [4]. However, at temperatures above 300 °C the NO_x conversion showed an obvious increase, which was due to the inhibition effect of H_2O on the unselective oxidation of NH_3. This point of view could be verified by the decrease of NH_3 conversion and enhancement of N_2 selectivity in the SCR reaction over $Fe_{0.75}Mn_{0.25}TiO_x$ in the presence of H_2O (see Fig. S3 in Supporting Information). For the reaction condition containing CO, CO_2 and H_2O, the SCR activity was very similar as that in the presence of H_2O alone, with the NO_x conversion keeping at 100% from 200 to 350 °C.

3.1.4. NO and NH_3 oxidation activities of $Fe_aMn_{1-a}TiO_x$ catalysts

It was reported that the enhancement of NO oxidation to NO_2 over SCR catalysts could significantly promote the low temperature activity due to the occurrence of the "fast SCR": $NO + NO_2 + 2NH_3 \rightarrow 2N_2 + 3H_2O$ [16,27,28]. The effect of NO_2 and the detailed "fast SCR" reaction mechanism have been studied extensively over conventional V_2O_5–WO_3/TiO_2 and Fe-zeolite catalysts (such as Fe/HBEA and Fe/ZSM-5) by many researchers [4,29–33]. In this study, the effect of Mn substitution amounts on NO oxidation activity of iron titanate catalyst was also investigated and the results are shown in Fig. 4A. With the increasing of Mn substitution amounts the NO conversion to NO_2 showed an obvious enhancement, and the maximum conversions were obtained when the substitution amount was above 0.5. Although the NO oxidation activities of $Fe_{0.2}Mn_{0.8}TiO_x$ and $MnTiO_x$ were much higher than that of $Fe_{0.75}Mn_{0.25}TiO_x$, the SCR activities over the former two catalysts were still a little lower than that over the latter one, as shown in Fig. 2. This implies that the SCR activity over these catalysts is not only related with the NO oxidation activity, but also related with some other structural or redox properties, which will be discussed later in this paper.

Previous study by Roy et al. [17] showed that the N_2 selectivity in the SCR reaction had a strong inverse correlation with the oxidation of NH_3, therefore the separate NH_3 oxidation experiments were also conducted over $Fe_aMn_{1-a}TiO_x$ catalysts. As shown in Fig. 4B, the NH_3 conversions had an obvious enhancement with the increasing of Mn substitution amounts, and the highest NH_3 conversions were obtained when the substitution amount was above 0.5. However, the N_2 selectivity showed an obvious decrease in NH_3 oxidation reactions at the same time (see Fig. S4 in Supporting Information), which is in accordance with the changing trend of N_2 selectivity in the SCR reactions. This implies that although the NO oxidation activity is enhanced when partial Fe is substituted by Mn which is beneficial to the promotion of SCR activity, the unselective oxidation of NH_3 to N_2O, NO or NO_2 in the SCR conditions is also enhanced, resulting in the production of a large amount of by-products. There should be a compromise of the SCR activity and N_2 selectivity when we determine on the Mn substitution amount in practical application.

3.2. Structural properties

3.2.1. N_2 physisorption

Fig. 5A shows the pore size distributions of $Fe_aMn_{1-a}TiO_x$ catalysts derived from the desorption branches of N_2 adsorption–desorption isotherms. In the diameter range below 3 nm, the N_2 adsorbed volume per gram per nm increased in the following sequence: $FeTiO_x < MnTiO_x < Fe_{0.2}Mn_{0.8}TiO_x < Fe_{0.75}Mn_{0.25}TiO_x < Fe_{0.5}Mn_{0.5}TiO_x$. This means that the $Fe_{0.5}Mn_{0.5}TiO_x$ sample has the most abundant micropores or mesopores, which can supply more inner surface area for the occurrence of SCR reaction. The BET surface areas in Fig. 5B also followed such a sequence, which is in well harmony with the sequence of SCR activity. The results in Fig. 5C show that $Fe_{0.5}Mn_{0.5}TiO_x$ possesses the largest pore volume due to the coexistence of iron and manganese species with the molar ratio of Fe:Mn being 1:1, which is beneficial to the enhancement of SCR

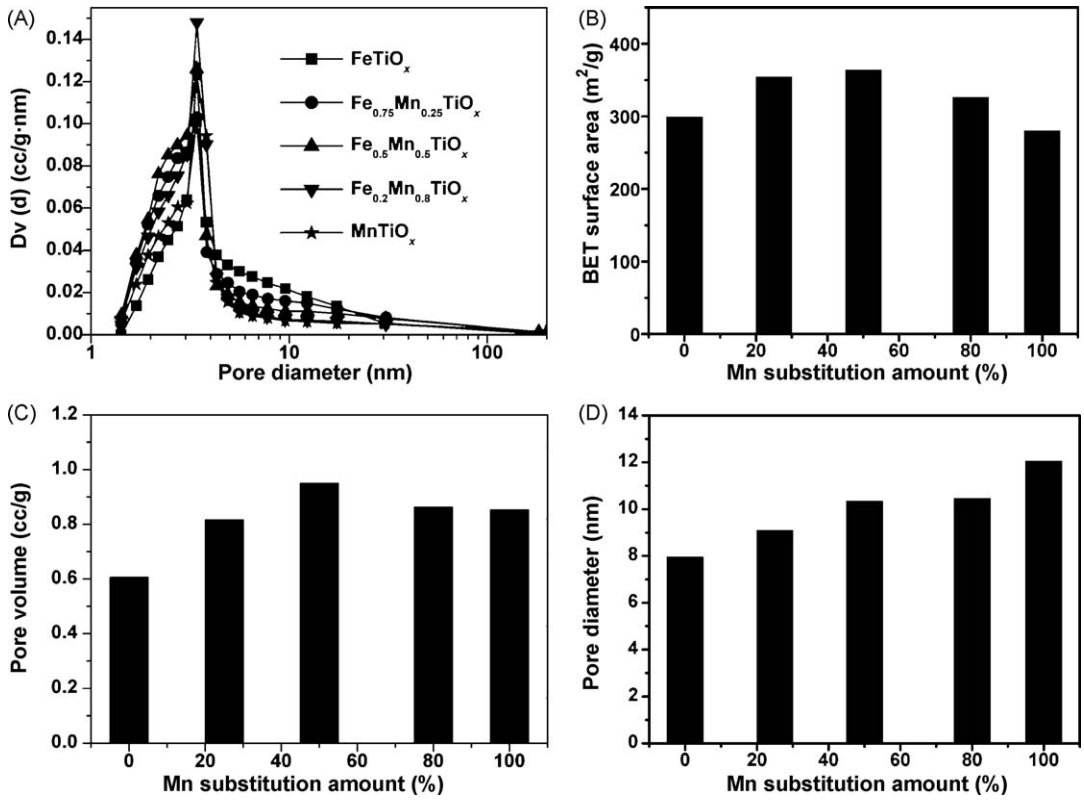

Fig. 5. N_2 adsorption–desorption results of $Fe_aMn_{1-a}TiO_x$ catalysts: (A) pore size distributions; (B) BET surface areas; (C) pore volumes; (D) average pore diameters.

activity. With the increasing of Mn substitution amounts, the average pore diameter in Fig. 5D became larger, which might be one of the reasons for the activity decline over $Fe_{0.2}Mn_{0.8}TiO_x$ and $MnTiO_x$.

3.2.2. XRD

Fig. 6 shows the XRD results of $Fe_aMn_{1-a}TiO_x$ catalysts together with the standard cards of $FeTiO_3$, $MnTiO_3$ and $FeMnTiO_4$ in JCPDS (vertical lines). All of the samples showed no obvious diffraction patterns besides some broad bumps, implying that all samples were in poor crystallization. The interaction between iron, manganese and titanium species led to a highly dispersive state of active phases, without forming iron oxides, manganese oxides or titanium oxide particles. In our previous study [5,6], we have concluded that the $FeTiO_x$ catalyst was mainly in the form of crystallite phases of Fe_2TiO_5 and $FeTiO_3$ with specific Fe–O–Ti structure which showed high SCR activity. The substitution of Fe by Mn did not destroy the crystallite structures; furthermore, some crystallites with Mn–O–Ti and Fe–O–Mn structures might also be formed, because either $FeMnTiO_4$ or $MnTiO_3$ also has some diffraction peaks in the positions of the broad bumps. The formation of new active phases might be another reason for the activity improvement.

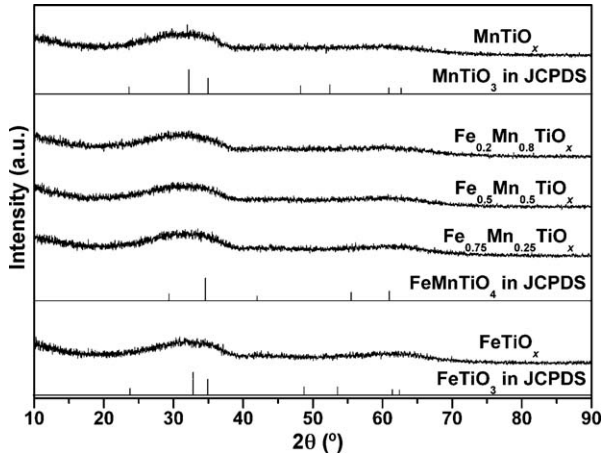

Fig. 6. XRD results of $Fe_aMn_{1-a}TiO_x$ catalysts and standard cards in JCPDS.

3.2.3. XAFS

For our $Fe_aMn_{1-a}TiO_x$ catalysts in crystallite phases, XAFS is a suitable tool to characterize the structural information because it can be used to determine the local environment around specific atoms, irrespective of crystallinity or dimensionality of the target materials. Fig. 7A presents the normalized XANES of Fe-K-edge in Fe-containing catalysts. All samples showed characteristic pre-edge peaks at 7114 eV, which could be attributed to 1s–3d dipolar forbidden transition [34]. The peak position and the peak shape corresponded well with those of the ferric compounds in fourfold or fivefold coordination [35], indicating that the iron species in our catalysts was mainly in Fe^{3+} oxidation state. It is reported that this pre-edge peak will get additional intensity if the iron center is in a noncentral symmetric environment or through mixing of 3d and 4p orbitals, which is caused by the breakdown of inversion symmetry because of the structure distortion (i.e. bond-angle disorder) [34,36]. As the XANES spectra in this study have been shifted vertically for comparison, we can directly read the pre-edge peak intensities by subtracting the base line values from the peak values. The inserted figure is the enlargement of the spectra region denoted by the dashed rectangle to better discriminate the pre-edge peak intensities. For $Fe_{0.5}Mn_{0.5}TiO_x$ catalyst, the intensity of the pre-edge peak was largest, implying that when the molar ratio of Fe:Mn is 1:1, the interaction between these two species led to a severest structure distortion of Fe–O coordination. Fig. 7C presents the normalized XANES of Mn-K-edge in Mn-containing catalysts and all samples showed characteristic pre-edge peaks at 6541 eV,

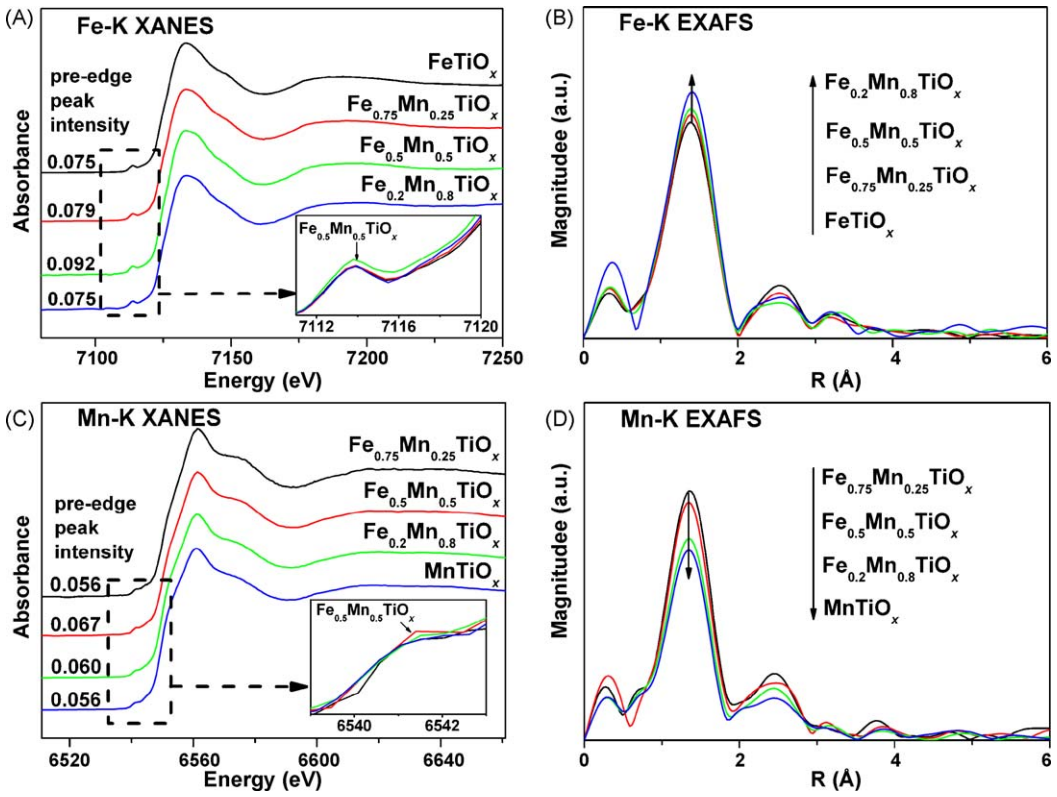

Fig. 7. (A) XANES, (B) FT-EXAFS results of Fe-K-edge and (C) XANES, (D) FT-EXAFS results of Mn-K-edge in $Fe_aMn_{1-a}TiO_x$ catalysts.

which could also be attributed to the crystal field transition from the core 1s levels to the empty 3d levels and more or less 4p hybridized by manganese ligands [37]. $Fe_{0.5}Mn_{0.5}TiO_x$ catalyst also had the largest intensity of pre-edge peak which can be distinguished from the inserted figure, suggesting a severest structure distortion of Mn–O coordination. It was reported that amorphous or crystallite materials with enormous structure distortion would provide more active sites for catalytic reactions than crystalline materials, which was probably responsible for the high catalytic activity. The amorphous MnO_x as electrocatalyst by Yang and Xu for oxygen reduction reaction is one of these examples [38]. Shishido et al. also concluded that the isolated and tetrahedrally coordinated iron sites with higher degree of structure distortion in the framework of Fe-MCM-41 were responsible for the high activity in oxidation reaction, while small iron oxide clusters with lower degree of structure distortion were not effective [39]. Therefore, we can deduce that the severest distortion of Fe–O and Mn–O coordination structure in our crystallite $Fe_{0.5}Mn_{0.5}TiO_x$ catalyst is also an important reason for its highest SCR activity.

The radial distribution function (R space, phase shift uncorrected) of Fe-K-edge and Mn-K-edge derived from the EXAFS data are shown in Fig. 7B and D, respectively. For Fe-K-edge, a peak centered at 1.41 Å showed up, which could be attributed to the first Fe–O shell. No obvious peak above 2 Å belonging to the second coordination shell was observed, indicating that all samples were in crystallite phase, which is in accordance with the XRD results. For Mn-K-edge, the situation was similar. Only one obvious peak at 1.35 Å due to the first Mn–O shell was observed, and the second coordination shell was not well crystallized, either. With the increasing of Mn substitution amounts, the peak intensity of Fe–O shell showed a monotonic increase, and at the same time the peak intensity of Mn–O shell showed a monotonic decrease. If we assume that the coordination numbers of Fe–O and Mn–O shells do not change during the Mn substitution process, the peak intensity in R space will only be relevant with the structural disorder (i.e. bond-length disorder). Lower peak intensity indicates higher degree of structural disorder. It was reported that the more disordering of the structure, the higher catalytic activity would be obtained over catalysts for various reactions, such as over the Cu/ZrO_2 catalyst for the steam reforming of methanol [40], the Ni–Co–B amorphous catalyst for the hydrogenation of benzene [41] and the mixed La–Sr–Co–Fe–O perovskite catalyst for the CO oxidation [42]. Although no direct correlation between the structural disorder and catalytic activity over SCR catalysts was clearly proposed by other researchers, some experimental results from literature showed that this empirical conclusion might also be applicable to the catalysts for the SCR reaction. For example, the iron species in Fe/ZSM-5 with more distorted tetrahedrally coordinated structure showed higher activity than that with regular octahedrally coordinated structure in the catalytic reduction of NO with *iso*-butane [43]. Moreover, the zeolite encapsulated vanadium oxo species [44] and the highly isolated vanadium species in mesoporous V_2O_5–TiO_2–SiO_2 catalyst [45] with distorted tetrahedrally coordinated structure also showed high activity in the SCR of NO with NH_3. In this study, both of the iron species and manganese species in our catalysts contributed to the SCR activity, and there was an inverse correlation between the structure distortion of Fe–O shell and Mn–O shell during the Mn substitution process. Summarizing the results in Fig. 7B and D, $Fe_{0.5}Mn_{0.5}TiO_x$ catalyst had the most appropriate structural disorder of these two active species, and this is another important reason for its highest SCR activity.

3.3. Redox properties

3.3.1. XPS

The XPS results of Fe 2p are shown in Fig. 8A. Two characteristic peaks ascribed to Fe $2p_{3/2}$ at 711.4 eV and Fe $2p_{1/2}$ at 724.9 eV appeared for each Fe-containing sample, indicating that the iron

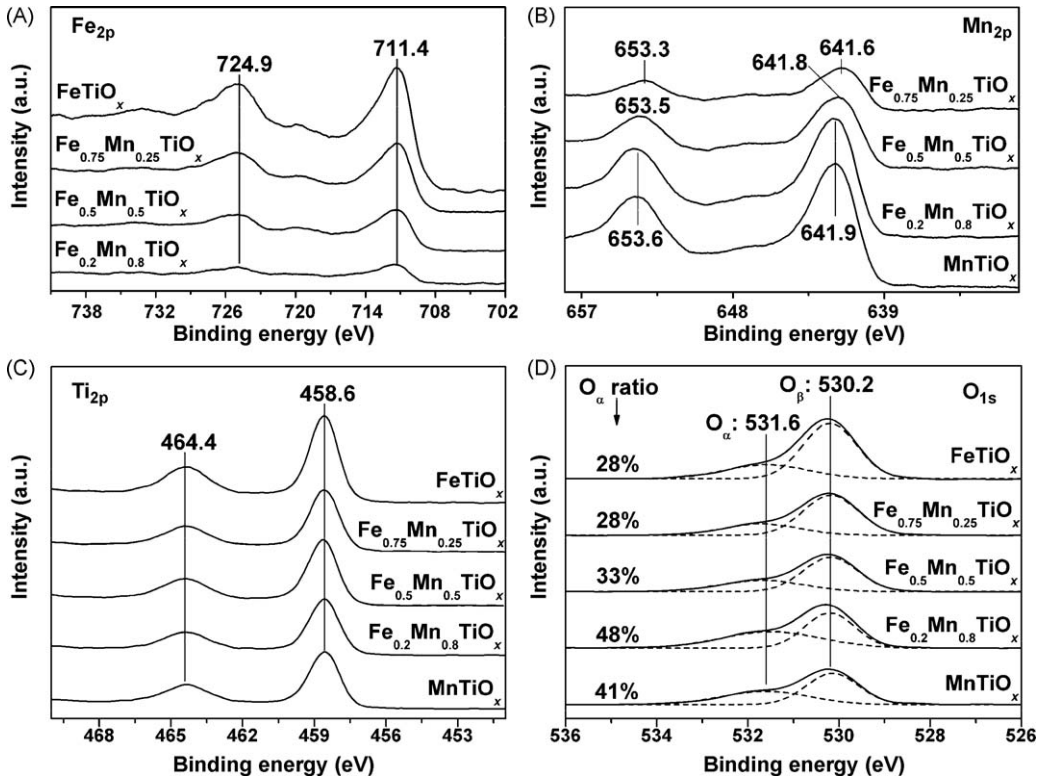

Fig. 8. XPS results of (A) Fe 2p, (B) Mn 2p, (C) Ti 2p and (D) O 1s in $Fe_aMn_{1-a}TiO_x$ catalysts.

species in these samples was in Fe^{3+} oxidation state [46]. It was reported in our previous study that the iron species in iron titanate catalyst possessed higher binding energies than that in pristine Fe_2O_3 due to the strong interaction between iron and titanium species [6], and the substitution of partial Fe by Mn did not change this situation. The iron species with enhanced oxidative ability than that in Fe_2O_3 was still responsible for the high SCR activity. With the increasing of Mn substitution amounts, the intensities of Fe $2p_{3/2}$ and Fe $2p_{1/2}$ peaks gradually decreased owing to the concentration reduction of surface iron species. However, the corresponding binding energies did not show variation, implying that the differences of SCR, NO oxidation and NH_3 oxidation activities over these catalysts were not caused by the redox ability change of iron species.

The XPS results of Mn 2p in Mn-containing samples are shown in Fig. 8B. For $Fe_{0.75}Mn_{0.25}TiO_x$ catalyst with low Mn substitution amount, the binding energies of Mn $2p_{3/2}$ and Mn $2p_{1/2}$ peaks were located at 641.6 and 653.3 eV, respectively, which indicated that the majority of manganese species in this sample was in Mn^{3+} oxidation state, similar as that in Mn_2O_3 [47,48]. Besides, a small fraction of manganese species in this sample was in Mn^{4+} oxidation state, thus the overall manganese species in $Fe_{0.75}Mn_{0.25}TiO_x$ showed a little higher binding energies than those in Mn_2O_3 which was reported in literature (Mn $2p_{3/2}$ at 641.2 ± 0.2 eV) [47]. With the increasing of Mn substitution amounts, the intensities of Mn $2p_{3/2}$ and Mn $2p_{1/2}$ peaks gradually enhanced due to the concentration increase of surface manganese species. At the same time, the corresponding binding energies also showed variation, with Mn $2p_{3/2}$ shifting from 641.6 to 641.9 eV and Mn $2p_{1/2}$ shifting from 653.3 to 653.6 eV. This result showed that the Mn^{4+}/Mn^{3+} ratio in $Fe_aMn_{1-a}TiO_x$ serial catalysts became larger when the Mn substitution amount was higher. With the increasing of Mn^{4+}/Mn^{3+} ratio, the oxidation of NO to NO_2 would get enhanced, which was beneficial to promote the low temperature SCR activity [49]. This is in accordance with the NO oxidation results in Fig. 4A. At the same time, the unselective oxidation of NH_3 would also get enhanced with the increasing of Mn^{4+}/Mn^{3+} ratio resulting in low N_2 selectivity in the SCR reaction, which was caused by the higher degree of hydrogen abstraction from ammonia by manganese species with higher oxidation state [7]. This is in accordance with the NH_3 oxidation results in Fig. 4B and Fig. S4.

Fig. 8C shows the XPS results of Ti 2p in all catalysts. For each sample, two characteristic peaks attributed to Ti $2p_{3/2}$ at 458.6 eV and Ti $2p_{1/2}$ at 464.4 eV showed up, indicating the presence of Ti^{4+} [50]. As the XPS results shown in our previous study [6], the binding energies of Ti $2p_{3/2}$ and Ti $2p_{1/2}$ in $FeTiO_x$ were smaller than those in pristine TiO_2 due to the strong interaction between iron and titanium species. This phenomenon was probably caused by the deviation of electronic cloud from Fe^{3+} to Ti^{4+}, because Ti^{4+} shows stronger affinity of electrons comparing with that of Fe^{3+}. Similar phenomenon was also observed on other iron–titanium oxide composites prepared by other researchers [51,52]. In this study, the introduction of manganese species did not influence the redox behavior of titanium species, because the Ti 2p peak positions showed no obvious change with the increasing of Mn substitution amounts.

Summarizing the XPS results of Fe 2p, Mn 2p and Ti 2p, we can conclude that the enhanced oxidative ability of $Fe_aMn_{1-a}TiO_x$ catalysts was mainly caused by the introduction of Mn, which showed higher oxidation state when the substitution amount was larger. We can infer that the adsorption of NO_x over these catalysts will get enhanced due to the higher surface concentration and stronger oxidative ability of manganese species. This point of view will be verified in the following experimental sections concerning NO_x adsorption abilities.

As the XPS results shown in Fig. 8D, the O 1s peak was fitted into two peaks by searching for the optimum combination of Gaussian bands with the correlation coefficients (r^2) above 0.99. The peak at 530.2 eV corresponds to the lattice oxygen O^{2-} (denoted as O_β), and the one at 531.6 eV corresponds to the surface adsorbed

oxygen (denoted as O_α) such as O_2^{2-} or O^- belonging to defect-oxide or hydroxyl-like group [49,53]. The surface chemisorbed oxygen O_α was reported to be highly active in oxidation reaction due to its higher mobility than lattice oxygen O_β [53,54], and the high relative concentration ratio of $O_\alpha/(O_\alpha + O_\beta)$ on catalyst surface could be correlated with high SCR activity [49]. After the Fe was substituted by Mn, the $O_\alpha/(O_\alpha + O_\beta)$ ratio had an obvious increase, especially at high Mn substitution amounts. This implies that comparing with $FeTiO_x$, there are more oxide defects or hydroxyl-like groups in Mn-containing catalysts. On one hand, the oxide defects can adsorb and activate gaseous O_2 to form active oxygen species, which is beneficial to promote the NO oxidation to NO_2 and thus the "fast SCR" process. On the other hand, the NH_3 adsorption in the form of NH_4^+ can also be enhanced due to the production of larger amount of surface hydroxyl groups, which act as Brønsted acid sites. The formed NH_4^+ can react with adsorbed NO_2 to produce active intermediate species, and then further react with gaseous NO to produce N_2 and H_2O [26,55,56]. The enhancement of NO_x and NH_3 adsorption over Mn substituted catalysts will be discussed later.

3.3.2. H_2-TPR

The above XPS results of O 1s could supply some information about the surface chemisorbed oxygen O_α over these catalysts, and the H_2-TPR results could supply some information about the total reducible oxygen including O_α and partial O_β. All H_2 consumption peaks shown in Fig. 9 could be attributed to the reduction of iron and manganese species, because the pristine TiO_2 sample showed no reduction peaks during the whole temperature range that we investigated [6,9].

In our previous study, we have concluded that the reduction of iron species in $FeTiO_x$ followed a two step process: Fe^{3+}–O–Ti → $Fe^{2+/3+}$–O–Ti → Fe^{2+}–O–Ti [6] with a T_{max} peak locating at 414 °C. After Mn substitution, the reduction process of iron species did not change, and the whole TPR profiles of $Fe_aMn_{1-a}TiO_x$ catalysts were composed of Fe and Mn reduction peaks. With the increasing of Mn substitution amounts, a low temperature reduction peak (T_1) between 350 and 400 °C showed up, which must be caused by the reduction of manganese species. This means that the oxygen mobility was greatly enhanced due to the introduction of Mn, which was beneficial to the SCR reaction. $Fe_{0.5}Mn_{0.5}TiO_x$ exhibited the lowest temperature of T_1 peak at 352 °C and this in harmony with its highest SCR activity. For $Fe_{0.2}Mn_{0.8}TiO_x$ and $MnTiO_x$ samples with higher Mn substitution amounts, another two well defined reduction peaks locating at relative high temperatures also emerged (T_2 at 480 or 544 °C, T_3 at 554 or 608 °C). Previous studies [9,57] showed that the reduction of pristine MnO_x or MnO_x/TiO_2 samples followed a two step process $MnO_2 \rightarrow Mn_2O_3 \rightarrow MnO$ or a three step process $MnO_2 \rightarrow Mn_2O_3 \rightarrow Mn_3O_4 \rightarrow MnO$, during which the area ratio of H_2 consumption peaks should be 1:1 or 3:1:2. However, the reduction process of our $MnTiO_x$ sample was not similar as either of these. The area ratio of $T_1/(T_2 + T_3)$ was calculated to be nearly 2:1, which implied that the T_1 reduction peak was due to Mn^{4+}–O_x–Ti → $Mn^{3+/2+}$–O_x–Ti. Herein, the manganese species in $Mn^{3+/2+}$–O_x–Ti intermediate had similar oxidation state as that in Mn_3O_4. Both of the T_2 and T_3 reduction peaks were ascribed to $Mn^{3+/2+}$–O_x–Ti → Mn^{2+}–O_x–Ti, because further reduction to metallic Mn^0 does not proceed until over 1200 °C [58]. Over the Mn-MCM-41 sample prepared by Reddy et al., the Mn^{4+} species was also only reduced to Mn^{2+} by H_2 at around 600 °C [59]. Therefore, in our $MnTiO_x$ sample after the T_2 reduction peak the majority of manganese species was in Mn^{2+} state, resulting in the formation of analogous pyrophanite ($Mn^{2+}TiO_3$) compound in the presence of Ti^{4+} species. This pyrophanite compound would possibly be sintered to form compact oxide layer on the catalyst surface and make it difficult for the gaseous H_2 to diffuse into the inner bulk phase, thus leading to the delayed appearance of the small T_3 reduction peak. The total reduction process of $MnTiO_x$ is similar as the results over MnO_x or MnO_x/Al_2O_3 in previous studies [7,60,61]. Moreover, it is noteworthy that the T_2 peak in $MnTiO_x$ delayed ca. 60 °C than that over $Fe_{0.2}Mn_{0.8}TiO_x$ and ca. 100 °C than that over $Fe_{0.5}Mn_{0.5}TiO_x$, which was mainly due to the absence of iron species. During the reduction process of iron and manganese containing catalysts, a small fraction of iron species was firstly reduced to metallic Fe^0 nanoparticles, which could dissociate H_2 into H atoms; in the presence of the in situ formed water vapor, the dissociated H atoms could be transferred effectively to further reduce the manganese oxides through the so-called H-spillover effect [62–64]. This H-spillover effect could significantly lower the reduction temperature of T_2 peak, which was a new feature introduced by the coexistence of iron and manganese species.

3.4. NH_3 and NO_x adsorption abilities

3.4.1. NH_3-TPD and NO_x-TPD

Fig. 10A shows the NH_3-TPD results over $Fe_aMn_{1-a}TiO_x$ catalysts using the fragments of $m/z = 16$ (NH_2) and $m/z = 15$ (NH) to identify NH_3 due to the disturbance of $m/z = 17$ by H_2O. In the temperature range from 30 to 500 °C, all of the samples showed three NH_3 desorption peaks. Comparing with the in situ DRIFTS results of NH_3-TPD in Fig. S5, we can assign these three peaks as

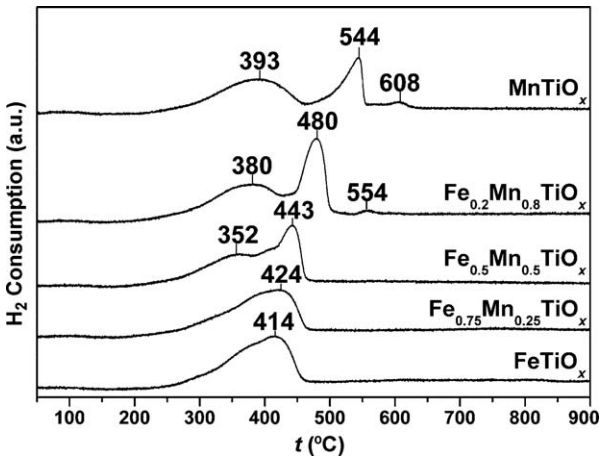

Fig. 9. H_2-TPR profiles of $Fe_aMn_{1-a}TiO_x$ catalysts.

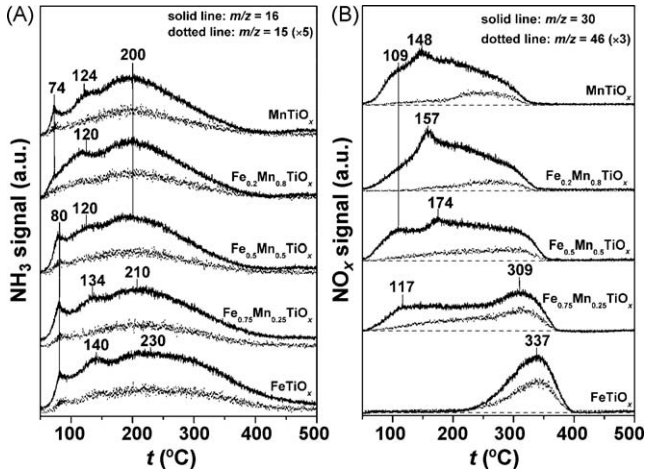

Fig. 10. TPD profiles of (A) NH_3 and (B) NO_x over $Fe_aMn_{1-a}TiO_x$ catalysts.

follows: the small sharp peaks below 100 °C were caused by the desorption of physisorbed NH_3; the medium-sized peaks between 120 and 140 °C were caused by the desorption of NH_4^+ weakly bound to surface hydroxyls; and the broadest peaks centered at 200–230 °C were caused by the desorption of coordinated NH_3 bound to Lewis acid sites and residual NH_4^+ strongly bound to surface hydroxyls with enhanced acidity by sulfate species (from $Ti(SO_4)_2$ precursor). Besides all the desorption peaks slightly moved to the low temperature edge, it seemed that the Mn substitution of Fe did not obviously influence the NH_3 adsorption ability of these catalysts, especially the adsorption amount. This result implied in an opposite way that NH_3 also mainly adsorbed on titanium sites over Mn substituted catalysts, similar as the situation that we described in previous study over $FeTiO_x$ catalyst [26]. The detailed relationship between surface adsorbed NH_3 species and SCR activity will be discussed in the following section.

The NO_x-TPD results over $Fe_aMn_{1-a}TiO_x$ catalysts are shown in Fig. 10B. Different from the NH_3-TPD results, the NO_x desorption profiles exhibited obvious change when partial Fe was substituted by Mn. Over unsubstituted $FeTiO_x$ catalyst, only one obvious NO_x desorption band centered at 337 °C showed up. With the increasing of Mn substitution amounts, there was a larger proportion of NO_x desorption from 100 to 300 °C. Comparing with the in situ DRIFTS results of NO_x-TPD in Fig. S6, we can have the peak assignments as follows: the peaks below 120 °C could be attributed to physisorbed NO_x; the peaks centered between 140 and 175 °C were due to the decomposition of monodentate nitrate species; and the broad peaks above 175 °C were due to the decomposition of bridging nitrate species and bidentate nitrate species with higher thermal stability. The dotted lines representing the fragment of desorbed NO_2 (m/z = 46) also confirmed this point of view. The introduction of Mn resulted in the enhanced NO oxidation to NO_2 and thus the enhanced adsorption of NO_x as nitrate species at lower temperatures. This means that comparing with the unsubstituted catalyst, more nitrate species on catalyst surface could participate in the SCR reaction in the temperature range that we investigated, which was beneficial to promote the SCR activity.

3.4.2. In situ DRIFTS of NH_3 and NO_x adsorption

The in situ DRIFTS results of NH_3 adsorption at 30 °C are shown in Fig. 11A. Over all samples, a weak and broad band centered at 1805 cm^{-1} was observed with similar intensity, which was difficult to be assigned due to the lack of literature support. Similar weak bands around 1800 cm^{-1} were also found on Fe–TiO_2–PILC catalyst after NH_3 adsorption at room temperature in Long and Yang's work [65]; however, they did not assign these bands probably due to the low surface concentration of these species. Considering the in situ DRIFTS results of NH_3-TPD in Fig. S5 and NH_3-TPD results in Fig. 10A, these NH_3 species showed rather low thermal stability and disappeared at ca. 100 °C, which might be ascribed to physisorbed NH_3. Over the catalyst surface with large surface area and strong acidity, these physisorbed NH_3 molecules might form ammonia clusters ($[NH_3]_n$) through the effect of hydrogen bonding in which N acted as electron couple donator and H from another NH_3 molecule nearby acted as electron couple receptor, thus exhibiting higher vibration frequency than that of gas phase NH_3. With the increasing of Mn substitution amounts in $Fe_aMn_{1-a}TiO_x$ serial catalysts, the bands attributed to NH_4^+ (δ_s at 1676 cm^{-1} and δ_{as} at 1458 cm^{-1}) [65–67] showed an obvious increase in intensity. The bands at 3020 and 2806 cm^{-1} attributed to N–H stretching vibration modes of NH_4^+ [66] also showed progressive increase in intensity. At the same time, the intensities of the negative bands at 3732 and 3676 cm^{-1} ascribed to O–H stretching vibration modes due to the interaction of surface hydroxyls with NH_3 also became larger during this Mn substitution process. This means that the introduction of Mn resulted in more Brønsted acid sites on the catalyst surface, which was favorable for the promotion of SCR activity. Schwidder et al. [68] also proposed a promoting effect of Brønsted acidity on the low temperature SCR activity over iron-based catalyst probably via an acid-catalyzed decomposition of active intermediate. The possible reason for the Brønsted acidity enhancement in this study might be that more residual sulfate species from $Ti(SO_4)_2$ precursor was left on the catalyst surface due to higher coordination ability of Mn^{4+} than that of Fe^{3+}. This point of view can be verified by the intensity increase of negative band around 1344 cm^{-1} attributed to the coverage of residual sulfate species ($\nu_{as\ S=O}$) [65] by adsorbed NH_3 with the increasing of Mn substitution amounts. For coordinated NH_3 bound to Lewis acid sites (δ_{as} at 1603 and δ_s at 1192 cm^{-1}), the band intensity firstly had an obvious increase, and then showed an intense decrease when the substitution amount was higher than 0.5. The bands at 3365, 3253 and 3160 cm^{-1} ascribed to N–H stretching vibration modes of coordinated NH_3 [66] also followed similar trend. It was reported that both ionic NH_4^+ and coordinated NH_3 could take part in the SCR process through reaction with NO_2 adsorbed species to form active intermediates [55]. Therefore, the proper proportion of Brønsted acid sites and Lewis acid sites over $Fe_{0.5}Mn_{0.5}TiO_x$ catalyst was responsible for its highest SCR activity.

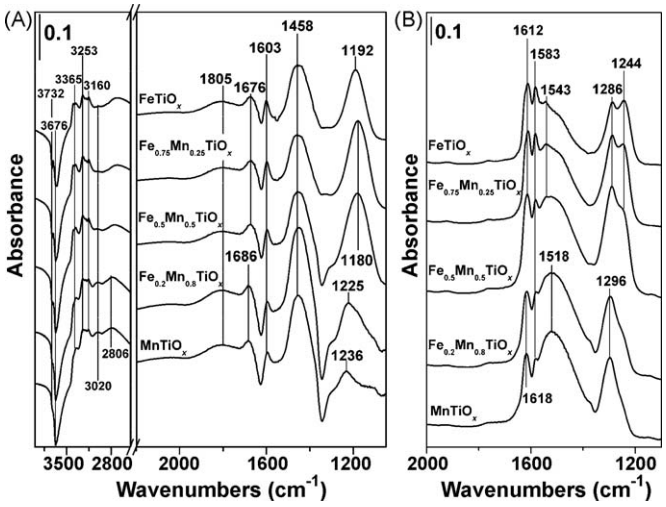

Fig. 11. In situ DRIFTS results of (A) NH_3 adsorption and (B) NO + O_2 adsorption over $Fe_aMn_{1-a}TiO_x$ catalysts at 30 °C.

Fig. 11B presents the in situ DRIFTS results of NO_x adsorption at 30 °C. With the increasing of Mn substitution amounts, the bands attributed to bridging nitrate species (ν_3 high at 1612 or 1618 cm^{-1} and ν_3 low at 1244 cm^{-1}) and bidentate nitrate species (ν_3 high at 1583 cm^{-1}) [69] showed no obvious change, except that the band at 1244 cm^{-1} in $Fe_{0.2}Mn_{0.8}TiO_x$ and $MnTiO_x$ was strongly overlapped by other growing nitrate species. This monotonously growing species was ascribed to monodentate nitrate (ν_3 high at 1543 or 1518 cm^{-1} and ν_3 low at 1286 or 1296 cm^{-1}) [69], which was thought to be the real reactive species in the SCR condition [26]. The higher Mn substitution amounts resulted in the enhancement of NO oxidation to NO_2, and thus the production of more monodentate nitrate species M–O–NO_2 (M = Fe and Mn), which was similar as the NO_2 adsorbed species in the previous study by Long and Yang [55]. In the SCR reaction condition, this M–O–NO_2 species could rapidly react with adjacent adsorbed NH_4^+ or NH_3 to produce more reactive intermediates M–O–$NO_2[NH_4^+]_2$ or M–O–$NO_2[NH_3]_2$, which could further react with gaseous NO to form N_2 and H_2O [55]. This reaction mechanism is very similar as the one proposed by other researchers, in which the reduction of ammonium nitrate by NO is an important step [30,32]. The in situ

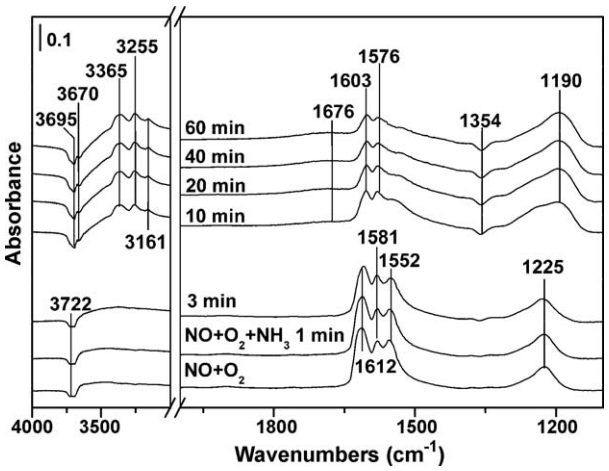

Fig. 12. In situ DRIFTS results of SCR reaction over $Fe_{0.75}Mn_{0.25}TiO_x$ catalyst at 200 °C, during which NO + O_2 was let in firstly and NH_3 was let in subsequently.

DRIFTS result of SCR reaction over $Fe_{0.75}Mn_{0.25}TiO_x$ in Fig. 12 also showed that the monodentate nitrate species (1552 cm^{-1}) could not be detected on the catalyst surface due to its high reactivity. Under the SCR reaction condition at 200 °C, only NH_3 adsorbed species (ionic NH_4^+ at 1676 cm^{-1} and coordinated NH_3 at 1603 and 1190 cm^{-1}) and inert bidentate nitrate species (1576 cm^{-1}) existed on the surface stably, implying the rapid consumption of reactive intermediates. Summarizing the in situ DRIFTS results of NH_3/NO_x adsorption in Fig. 11 and the SCR reaction in Fig. 12, on the $Fe_{0.5}Mn_{0.5}TiO_x$ catalyst the amount of NH_4^+ and NH_3 was the most abundant, and the formation of reactive monodentate nitrate species was also greatly enhanced. Therefore, it was reasonable to obtain the highest SCR activity over this catalyst.

4. Conclusions

The substitution of partial Fe by Mn could significantly promote the SCR activity of iron titanate catalyst, especially in the low temperature range. $Fe_{0.5}Mn_{0.5}TiO_x$ with the molar ratio of Fe:Mn = 1:1 showed the best activity, over which NO_x was totally eliminated at 175 °C at GHSV = 50 000 h^{-1}. However, the N_2 selectivity showed an obvious decrease with the increasing of Mn substitution amounts, and there should be a compromise between the SCR activity and N_2 selectivity when we determine on the Mn substitution amount in practical industrial application.

The active phases in Mn substituted catalysts were still in crystallite states, similar as those in iron titanate catalyst. The strong interaction of iron, manganese and titanium species in $Fe_{0.5}Mn_{0.5}TiO_x$ resulted in the largest surface area and porosity, the severest structural distortion and most appropriate structural disorder, the enhanced oxidative ability of manganese species, the highest mobility of lattice oxygen, the proper ratio of Brønsted acid sites and Lewis acid sites together with the enhanced NO_x adsorption capacity, which were all responsible for its highest SCR activity. Studies concerning the SCR reaction mechanism, origin of N_2O by-product and H_2O/SO_2 inhibition effect over Mn substituted catalyst are under way.

Acknowledgements

We sincerely appreciate the help from National Synchrotron Radiation Laboratory, University of Science and Technology of China for supplying the beam time to carry out XAFS experiments. This work was financially supported by Chinese Academy of Sciences (KZCX1-YW-06-04) and the National High Technology Research and Development Program of China (2006AA06A304, 2009AA06Z301).

Appendix A. Supplementary data

Supplementary data associated with this article can be found, in the online version, at doi:10.1016/j.apcatb.2009.09.029.

References

[1] H. Bosch, F. Janssen, Catal. Today 2 (1988) 369.
[2] G. Busca, L. Lietti, G. Ramis, F. Berti, Appl. Catal. B: Environ. 18 (1998) 1.
[3] J.P. Dunn, P.R. Koppula, H.G. Stenger, I.E. Wachs, Appl. Catal. B: Environ. 19 (1998) 103.
[4] P. Balle, B. Geiger, S. Kureti, Appl. Catal. B: Environ. 85 (2009) 109.
[5] F. Liu, H. He, C. Zhang, Chem. Commun. (2008) 2043.
[6] F. Liu, H. He, C. Zhang, Z. Feng, L. Zheng, Y. Xie, T. Hu, Appl. Catal. B: Environ., submitted for publication.
[7] F. Kapteijn, L. Singoredjo, A. Andreini, J.A. Moulijn, Appl. Catal. B: Environ. 3 (1994) 173.
[8] X. Tang, J. Hao, W. Xu, J. Li, Catal. Commun. 8 (2007) 329.
[9] P.R. Ettireddy, N. Ettireddy, S. Mamedov, P. Boolchand, P.G. Smirniotis, Appl. Catal. B: Environ. 76 (2007) 123.
[10] Z. Wu, B. Jiang, Y. Liu, Appl. Catal. B: Environ. 79 (2008) 347.
[11] P.G. Smirniotis, P.M. Sreekanth, D.A. Peña, R.G. Jenkins, Ind. Eng. Chem. Res. 45 (2006) 6436.
[12] T. Grzybek, J. Pasel, H. Papp, Phys. Chem. Chem. Phys. 1 (1999) 341.
[13] G. Qi, R.T. Yang, R. Chang, Appl. Catal. B: Environ. 51 (2004) 93.
[14] F. Eigenmann, M. Maciejewski, A. Baiker, Appl. Catal. B: Environ. 62 (2006) 311.
[15] M. Kang, E.D. Park, J.M. Kim, J.E. Yie, Catal. Today 111 (2006) 236.
[16] G. Qi, R.T. Yang, Appl. Catal. B: Environ. 44 (2003) 217.
[17] S. Roy, B. Viswanath, M.S. Hegde, G. Madras, J. Phys. Chem. C 112 (2008) 6002.
[18] G. Qi, R.T. Yang, R. Chang, S. Cardoso, R.A. Smith, Appl. Catal. A: Gen. 275 (2004) 207.
[19] G. Carja, G. Delahay, C. Signorile, B. Coq, Chem. Commun. (2004) 1404.
[20] M. Casanova, E. Rocchini, A. Trovarelli, K. Schermanz, I. Begsteiger, J. Alloys Compd. 408–412 (2006) 1108.
[21] S. Kieger, G. Delahay, B. Coq, Appl. Catal. B: Environ. 25 (2000) 1.
[22] X. Wang, T. Zhang, X. Sun, W. Guan, D. Liang, L. Lin, Appl. Catal. B: Environ. 24 (2000) 169.
[23] K.V. Klementev, J. Phys. D: Appl. Phys. 34 (2001) 209.
[24] R.Q. Long, R.T. Yang, J. Catal. 188 (1999) 332.
[25] J.-H. Park, H.J. Park, J.H. Baik, I.S. Nam, C.-H. Shin, J.-H. Lee, B.K. Cho, S.H. Oh, J. Catal. 240 (2006) 47.
[26] F. Liu, H. He, C. Zhang, Appl. Catal. B: Environ., submitted for publication.
[27] G. Madia, M. Koebel, M. Elsener, A. Wokaun, Ind. Eng. Chem. Res. 41 (2002) 3512.
[28] R.Q. Long, R.T. Yang, J. Catal. 198 (2001) 20.
[29] C. Ciardelli, I. Nova, E. Tronconi, D. Chatterjee, B. Bandl-Konrad, M. Weibel, B. Krutzsch, Appl. Catal. B: Environ. 70 (2007) 80.
[30] M. Devadas, O. Kröcher, M. Elsener, A. Wokaun, N. Söger, M. Pfeifer, Y. Demel, L. Mussmann, Appl. Catal. B: Environ. 67 (2006) 187.
[31] M. Koebel, G. Madia, M. Elsener, Catal. Today 73 (2002) 239.
[32] A. Grossale, I. Nova, E. Tronconi, D. Chatterjee, M. Weibel, J. Catal. 256 (2008) 312.
[33] M. Schwidder, S. Heikens, A. De Toni, S. Geisler, M. Berndt, A. Brückner, W. Grünert, J. Catal. 259 (2008) 96.
[34] Y. Wang, Q. Zhang, T. Shishido, K. Takehira, J. Catal. 209 (2002) 186.
[35] P.-E. Petit, F. Farges, M. Wilke, V.A. Solé, J. Synchrotron Radiat. 8 (2001) 952.
[36] T. Kawabata, N. Fujisaki, T. Shishido, K. Nomura, T. Sano, K. Takehira, J. Mol. Catal. A: Chem. 253 (2006) 279.
[37] E. Chalmin, F. Farges, G.E. Brown Jr., Contrib. Mineral. Petrol. 157 (2009) 111.
[38] J. Yang, J.J. Xu, Electrochem. Commun. 5 (2003) 306.
[39] T. Shishido, Q. Zhang, Y. Wang, T. Tanaka, K. Takehira, Phys. Scripta T115 (2005) 762.
[40] A. Szizybalski, F. Girgsdies, A. Rabis, Y. Wang, M. Niederberger, T. Ressler, J. Catal. 233 (2005) 297.
[41] B. Shen, S. Wei, K. Fang, J.F. Deng, Appl. Phys. A 65 (1997) 295.
[42] L.A. Isupova, V.A. Sadykov, S.V. Tsybulya, G.N. Kryukova, V.P. Ivanov, A.N. Petrov, O.F. Kononchuk, React. Kinet. Catal. Lett. 62 (1997) 129.
[43] M.S. Batista, M. Wallau, E.A. Urquieta-González, Braz. J. Chem. Eng. 22 (2005) 341.
[44] R.C. Adams, L. Xu, K. Moller, T. Bein, W.N. Delgass, Catal. Today 33 (1997) 263.
[45] V.I. Pârvulescu, S. Boghosian, V. Pârvulescu, S.M. Jung, P. Grange, J. Catal. 217 (2003) 172.
[46] T. Grzybek, J. Klinik, B. Buczek, Surf. Interface Anal. 23 (1995) 815.
[47] D.A. Peña, B.S. Uphade, P.G. Smirniotis, J. Catal. 221 (2004) 421.
[48] J. Li, J. Chen, R. Ke, C. Luo, J. Hao, Catal. Commun. 8 (2007) 1896.
[49] M. Kang, E.D. Park, J.M. Kim, J.E. Yie, Appl. Catal. A: Gen. 327 (2007) 261.
[50] S. Yuan, Q. Sheng, J. Zhang, H. Yamashita, D. He, Micropor. Mesopor. Mater. 110 (2008) 501.
[51] N. Perkas, O. Palchik, I. Brukental, I. Nowik, Y. Gofer, Y. Koltypin, A. Gedanken, J. Phys. Chem. B 107 (2003) 8772.
[52] A. Glisenti, J. Mol. Catal. A: Chem. 153 (2000) 169.
[53] Z. Wu, R. Jin, Y. Liu, H. Wang, Catal. Commun. 9 (2008) 2217.

[54] H. Chen, A. Sayari, A. Adnot, F. Larachi, Appl. Catal. B: Environ. 32 (2001) 195.
[55] R.Q. Long, R.T. Yang, J. Catal. 190 (2000) 22.
[56] Z. Wu, B. Jiang, Y. Liu, H. Wang, R. Jin, Environ. Sci. Technol. 41 (2007) 5812.
[57] A. Khan, P.G. Smirniotis, J. Mol. Catal. A: Chem. 280 (2008) 43.
[58] J. Carnö, M. Ferrandon, E. Björnbom, S. Järås, Appl. Catal. A: Gen. 155 (1997) 265.
[59] E.P. Reddy, B. Sun, P.G. Smirniotis, J. Phys. Chem. B 108 (2004) 17198.
[60] X. Tang, Y. Li, X. Huang, Y. Xu, H. Zhu, J. Wang, W. Shen, Appl. Catal. B: Environ. 62 (2006) 265.
[61] M.C. Álvarez-Galván, V.A. de la Peña O'Shea, J.L.G. Fierro, P.L. Arias, Catal. Commun. 4 (2003) 223.
[62] O.J. Wimmers, P. Arnoldy, J.A. Moulijn, J. Phys. Chem. 90 (1986) 1331.
[63] R.P. Viswanath, B. Viswanathan, M.V.C. Sastri, React. Kinet. Catal. Lett. 2 (1975) 51.
[64] W.K. Jozwiak, E. Kaczmarek, T.P. Maniecki, W. Ignaczak, W. Maniukiewicz, Appl. Catal. A: Gen. 326 (2007) 17.
[65] R.Q. Long, R.T. Yang, J. Catal. 186 (1999) 254.
[66] N.Y. Topsøe, Science 265 (1994) 1217.
[67] G. Ramis, L. Yi, G. Busca, Catal. Today 28 (1996) 373.
[68] M. Schwidder, M.S. Kumar, U. Bentrup, J. Pérez-Ramírez, A. Brückner, W. Grünert, Micropor. Mesopor. Mater. 111 (2008) 124.
[69] G.M. Underwood, T.M. Miller, V.H. Grassian, J. Phys. Chem. A 103 (1999) 6184.